Distribution Agreement

In presenting this thesis or dissertation as a partial fulfillment of the requirements for an advanced degree from Emory University, I hereby grant to Emory University and its agents the non-exclusive license to archive, make accessible, and display my thesis or dissertation in whole or in part in all forms of media, now or hereafter known, including display on the world wide web. I understand that I may select some access restrictions as part of the online submission of this thesis or dissertation. I retain all ownership rights to the copyright of the thesis or dissertation. I also retain the right to use in future works (such as articles or books) all or part of this thesis or dissertation.

Signature:

Brett A. McGuire	Date

High Resolution THz Spectroscopy of Astrophysically Relevant Ions

By

Brett Andrew McGuire
Master of Science

Chemistry

Susanna L. Widicus Weaver, Ph.D.
Advisor

Joel M. Bowman, Ph.D.
Committee Member

Michael Heaven, Ph.D.
Committee Member

Accepted:

Lisa A. Tedesco, Ph.D.
Dead of the James T. Laney School of Graduate Studies

Date

High Resolution THz Spectroscopy of Astrophysically Relevant Ions

By

Brett Andrew McGuire
B.S., University of Illinois at Urbana-Champaign, 2009

Advisor: Susanna L. Widicus Weaver, Ph.D.

An abstract of
A thesis submitted to the Faculty of the
James T. Laney School of Graduate Studies of Emory University
in partial fulfillment of the requirements for the degree of
Master of Science
in Chemistry
2011

Abstract

High Resolution THz Spectroscopy of Astrophysically Relevant Ions
By Brett Andrew McGuire

Ions and radicals are thought to play fundamental roles in the complex chemistry of the interstellar medium (ISM). Identification of these species in interstellar environments hinges on the availability of accurate laboratory spectra with which to compare. The work presented here is focused on developing equipment and techniques to study these species, with an aim towards the eventual acquisition of the rotational spectrum of protonated methanol, an elusive organic ion that is thought to be central to gas-phase organic chemical processes in the ISM. Protonated methanol is a highly fluxional molecule, and this study will progress not only our knowledge of its effects on interstellar chemistry, but also our fundamental understanding of the intramolecular motion in organic molecules that guides reaction mechanisms. In order to achieve this goal, I have designed new supersonic expansion discharge sources that will favor protonation of organic molecules, combined these sources with multipass direct-absorption spectroscopy systems, and worked towards the development of a new, high-resolution, high-sensitivity spectrometer that operates in the terahertz (THz) range. I have also conducted numerous broadband spectral line surveys of a variety of interstellar sources to develop a catalog for rapid identification of new molecules as laboratory data becomes available.

High Resolution THz Spectroscopy of Astrophysically Relevant Ions

By

Brett Andrew McGuire
B.S., University of Illinois at Urbana-Champaign, 2009

Advisor: Susanna L. Widicus Weaver, Ph.D.

A thesis submitted to the Faculty of the
James T. Laney School of Graduate Studies of Emory University
in partial fulfillment of the requirements for the degree of
Master of Science
in Chemistry
2011

Acknowledgements

Thanks go first and foremost to my parents, who have encouraged my scientific career and education ever since my father set a batch of colored acid/base indicators in front of me and my mother helped me put a plastic bag over a tree branch to watch the condensation form. Their unwavering support through grade school, high school, undergraduate, and now graduate school has been invaluable, unequaled, and irreplaceable. Thanks guys! Second, to my advisor, Susanna, who encouraged me to try new things and step out of my comfort zone as a post doc at Illinois and who gave me remarkable opportunities to get my name out there in the community and engage others in my field as my graduate advisor. And thanks as well go to her group here at Emory, who have been fantastic colleagues, scientific collaborators, and friends. Special shout outs to the "old crowd" Jay Kroll, Mary Radhuber, and Jake Laas. And to the newbies as well, who I wish I had had more time to work with but, alas all good things must come to an end, Brian Hays and Blithe Rocher! My committee members, Joel Bowman and Michael Heaven, have been the best I could have asked for: people so smart, so kind, and so willing to help it's mind boggling!

It takes a special kind of person to put up with me, more so even if you choose to do it willingly! I will forever be indebted to my lab partner and best friend, Brandon Carroll. You're way smarter than me (and than you realize, I think) and you never failed to have an unlimited supply of witty (or not so witty) banter at the ready to lighten the mood. I would not have lasted six months, I think, without such a great friend around. You'll always have my deepest and most sincere gratitude for your friendship and your support.

Graduate school has been tough, but having a family here to laugh with, curse the gods of chemistry and physics with, and swear up and down about everything from classes to professors to taxes with has made the experience so much easier and made my life more enjoyable. To my family: Jen Bon, Caitlin & Mike Davis, and David

& Lisa Guptill: I'll miss you! Whether it be trivia nights, game nights, or Lord of the Rings marathons, I would have gone nuts without such a great group of people to support me as I worked through this research and thesis. You guys are the best!

Thanks go as well to the many people who have helped me throughout my two years here by lending their advice, their knowledge, or their sheer awesomeness. Ben McCall and Kyle Crabtree have never ceased to be wonderful resources of all three and I thank them for all their help since I left Illinois. Steve Krebs and Patti Barnett are beyond awesome, especially as they'll always tell you when you've done something silly! Ann Dasher of course has made everything here easier, from registering for classes to getting this thesis turned in and submitted, and always with a smile. Thanks to Stephenie Thioubou, Tim Stephens, and Marcus Rodriguez, for dealing with the red tape so I could deal with the research, and never complaining when I kept showing up with more stuff. And thanks to Cody Anderson, for producing such wonderful machine work from information provided from such an artistically and spatially challenge person (me!).

And lastly thanks to all of my friends and colleagues who have helped make me into the person and scientist I am today. I could fill the rest of this thesis with your names and praises, but as I should probably get to the science at some point I'll just have to say: Thank You!

Contents

List of Figures

List of Tables

1 Introduction

With the advent of new cutting-edge observatories that operate in the far-IR or the THz range, such as the Atacama Large Millimeter Array (ALMA) and the Herschel Space Observatory (HSO), the need for high-resolution rotational spectra of molecules in the millimeter and submillimeter range is necessary for full analysis of the observations. To date, nearly 160 molecules have been detected in interstellar space [1] and a significant fraction of these are ions and radicals. This fraction is most likely underrepresented, as the limited laboratory characterization of such species precludes identification of their lines in observational spectra. In fact a recent line survey of the star forming region Orion-KL shows only 43% (1285) of the observed lines identified in only a ∼28 GHz region [2]. Given their importance in interstellar chemical reactions, it is likely that some fraction of the unidentified lines arise from ions and radicals.

Reactive molecules are thought to be ubiquitous in, and play a major role in the chemistry of the interstellar medium (ISM). Before these hypotheses can be thoroughly tested, however, laboratory studies of such molecules must be conducted to allow identification of these species in observations of various interstellar environments. The work presented here is focused on acquiring the rotational spectrum of these molecules, with the ultimate goal of studying protonated methanol ($CH_3OH_2^+$), an elusive organic ion that is thought to be fundamental to gas-phase chemical processes in the ISM leading to complex organic chemistry. Protonated methnaol has long been thought to play a key role in the formation of complex organic molecules and prebiotic molecules in the ISM [3]. Fluxional species like protonated methanol are of fundamental interest in chemistry, as these systems have significant internal motion (rotation, torsion, and wagging motions) and as such offer a means to study these internal degrees of freedom and their effects on molecular structure and reac-

tivity. As such, this study will also progress our fundamental understanding of the intramolecular motion in organic molecules that guides reaction mechanisms.

Obtaining useful spectral information about these types of unstable species presents a number of experimental challenges. Production of species like protonated methanol through electrical (plasma) discharges, by far the most common method, is generally inefficient and highly energetic. This results in a low number density of target ions which are also generated at very high temperatures, greatly increasing the spectral complexity and weakening the intensity of observed spectral lines due to the increased partition function. This necessitates the use of a high-sensitivity spectroscopic technique in the target frequency range coupled with a method for cooling the target species. The work presented here has been focused on the development of sources to both produce and cool the target ions, as well as the development of high-resolution, high-sensitivity cavity ringdown spectrometer in the THz region with sufficient sensitivity to detect their rotational spectral signatures. The spectra gained from these studies will ultimately be used to guide searches for these molecules through observations of a variety of interstellar environments.

1.1 Laboratory Background

1.1.1 Supersonic Expansions

A method for producing and cooling unstable gas-phase species is required for the study of organic ions like protonated methanol. The most common technique for cooling energetic, gas-phase species is through the use of a supersonic expansion [6]. The incorporation of a supersonic expansion with a discharge source was first proposed by Engelking and associates [4, 5]. By expanding the ions after they are produced, they undergo an adiabatic cooling process which can lower their rotational temperatures to a few tens of Kelvin.

A well-proven design for supersonic expansions is based on the work of Campargue. Campargue-type expansions are characterized by gas expansion from a high pressure region to a lower pressure expansion chamber with pressures on the order of 10^{-2} to 1 torr. Such high pressures allow the expansion to interact with the background gas and create a "well-defined free-jet shock wave system" [7]. The formation of the barrel shock – a hot, turbulent region surrounding the center of the expansion – protects the molecules in the center from the background gas, creating a "zone of silence." Within this zone, the molecules behave as if they are entering a perfect vacuum, and a very high degree of cooling occurs. Background gas penetration into the zone of silence occurs at the Mach Disk, which is formed a distance X_M from the aperture as defined as $X_M = 0.67D\sqrt{P_0/P}$, where D is the diameter of the nozzle in μm, P_0 is the backing pressure in torr, and P is the pressure of the expansion chamber in torr. By expanding the length of the zone of silence as much as possible and thus increasing the time the molecules have for cooling, Campargue has shown achievable temperatures as low as 6 mK in the zone of silence [7]. As described in section 2.2, one focus of my initial work has been to develop supersonic expansion sources that favor the production of protonated ions.

1.1.2 Cavity Ringdown Spectroscopy

In addition to the need for a production method for ions, a high-sensitivity detection scheme is desirable. Traditional direct absorption experiments, relying on the Beer-Lambert Law, are limited by the accuracy with which the ratio of I to I_0 can be measured. The use of multi-pass setups, such as White cells [8] and Herriott cells [9] can alleviate some of these issues, but sensitivity is still limited. Such techniques require that each pass be separated in position space, creating a physical upper-limit to the number of passes possible for a setup, and thus the total path length [10]. Cavity ringdown spectroscopy (CRDS) represents an ideal solution to these problems,

providing both extremely long path lengths via a Fabry-Perot cavity [11] and the ability to measure absorption independent of variations in intensity.

The integration of this technique with continuous wave (cw) sources was first described by Romanini et al. [15]. A traditional cw-CRDS system consists of a confocal cavity formed by two very highly reflective mirrors separated by a distance equal or greater to their radii of curvature to form a stable resonator (see Figure 1). Radiation is generated, passed through mode-matching optics, and coupled into the cavity through the back of the first mirror. The cavity is then swept over a small distance, usually by use of a piezo-electric driver or motorized translation stage coupled with one of the mirrors. As a result, light will only build up in the cavity when the cavity length is such that the source frequency is on resonance with the cavity. When the cavity is on resonance, intensity is allowed to build up to a threshold value. The input radiation is then decoupled from the cavity, either by shutting off the source or via some form of switching, most commonly by use of an acousto-optic modulator (AOM). The cavity then rings down and the signal is observed as a decay through the back of the second mirror. The rate of decay of light in the cavity is directly proportional to the cavity loss. In an empty system, this is due mainly to the inperfect reflectivity of the mirrors and diffractive losses. If, however, an absorber is introduced

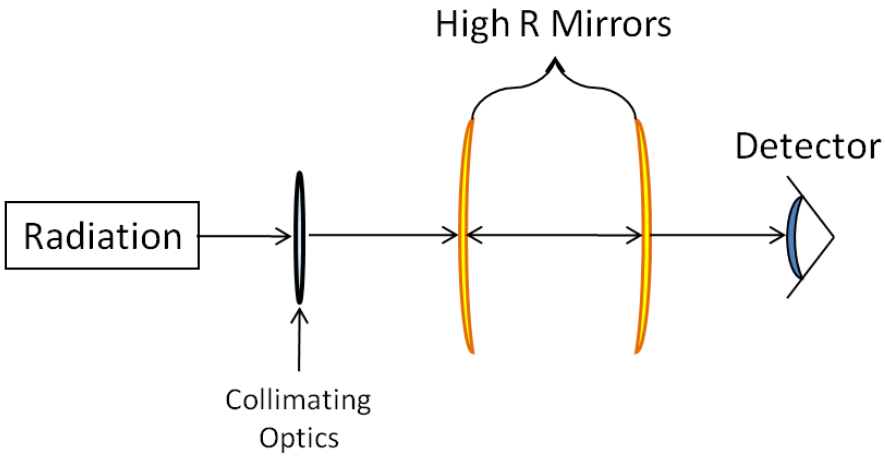

Figure 1: Basic setup of a cw-CRDS system.

into the cavity, the rate of decay is increased proportional to the absorbance of the species.

The decay signal out of the cavity is fit to determine the "time constant," or time it takes for the signal to decay to $1/e$ of its original value. The time constant can be well approximated as shown in Equation 1, where τ is the time constant, t_r is the round-trip time of light in the cavity, $(1 - R)$ is the loss due to the mirrors of reflectivity R, and $2\alpha l_s$ is the round-trip absorbance for a sample with absorption coefficient α and length l_s.

$$\tau = \frac{t_r}{2[(1 - R) + \alpha l_s]} \tag{1}$$

The values for t_r and R are properties of the system, and therefore the absorbance of the species in the cavity can be determined at each wavelength by measuring the time constant of the system. By scanning the input laser in frequency, an absorption spectrum of the species can be obtained.

CRDS offers several advantages over traditional multi-pass setups. First, the probe beam retraces itself over each pass, without the need to be spatially separated. This offers a huge advantage, as kilometers of pathlength can be achieved with a relatively small sample size. Second, because the measurement depends only on the rate of decay of the light, the measurement is virtually independent of variations in intensity, so long as the signal is sufficiently intense for detection.

2 Results and Discussion

2.1 THz Cavity Ringdown

Mirrors of sufficient reflectivity which also permit the transmission of light into and out of the cavity do not exist in the targeted THz region of the spectrum. An alternative approach is being developed in the Widicus Weaver group where the cavity is formed by two wire grid polarizers. These polarizers, when tuned to exactly 90° from the polarization of the radiation, serve as near perfect reflectors, with reflectivities $\sim 99.9\%$ achievable [12].

2.1.1 Initial Designs

The initial design for the system consisted of an off-axis cavity formed by two polarizers and a large, spherical silver mirror as shown in Figure 2a. The light was injected through the back of the first polarizer, refocused on each pass by the spherical mirror, and detected through the second polarizer, perpendicular to the incoming radiation. This setup presented a number of problems due to the complexity of the optical system. First, there is a lack of commercially available optical components, specifically lenses of appropriate diameter and size, in this frequency region. Those most readily available are 2 inch diameter teflon lenses with focal lengths of 100 mm, 300 mm, and 500 mm. This severely limits the options for constructing more complex optical systems, such as telescopes, to produce either a well-collimated beam or a beam with a specific radius of curvature required for coupling light into the CRDS cavity. Further, because of these limitations, the beam waist size is difficult to control and is in general quite large (on the order of 1 - 1.5 inches). As a result, setups requiring the isolation of two beams which are not spatially well-separated becomes exceedingly difficult.

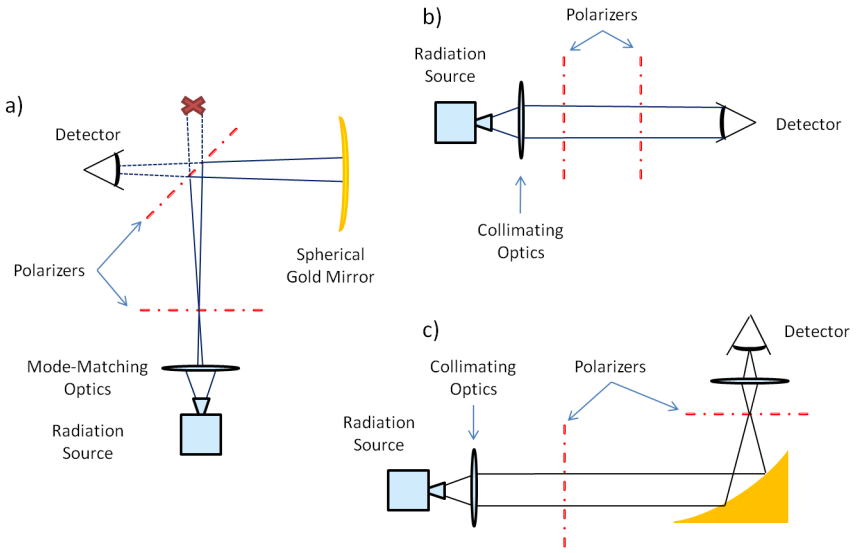

Figure 2: a) Off-axis design for the cavity. Beam path shown without divergence. b) Parallel polarizer setup. c) Off-axis cavity using an OAP.

As a simpler test of the ability of the polarizers to form a reflective cavity, the setup shown in Figure 2b was constructed. Although easier for alignment and detection, no cavity modes were detected with this setup. This was likely due to the lack of focusing elements within the cavity. Even a fairly well-collimated beam, after a sufficient number of round-trips within the cavity, would diverge to the point of overfilling the polarizers, resulting in losses beyond those from diffraction and deflection.

To combat this, and building on earlier work by Braakman [12], an off-axis paraboloid (OAP) was inserted into the middle of the cavity and the second polarizer was positioned at the focal point of the OAP (see Figure 2c). The radiation is focused by the OAP onto the second polarizer, reflects back, and is collimated as it returns to the first polarizer. On each successive pass, the radiation is refocused and re-collimated, precluding the beam from diverging and overfilling the polarizers and preventing the losses discussed above.

The first observation of cavity modes was accomplished with this configuration (see Fig 3). The regular spacing of the modes gives the free spectral range for the cavity of 454 MHz. The experimental length of the cavity can be calculated using

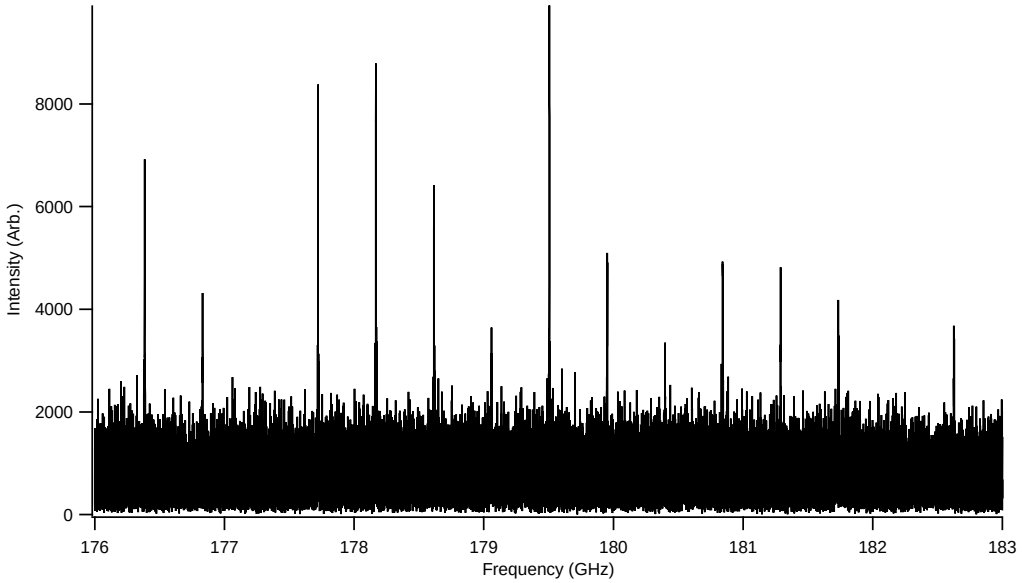

Figure 3: First detection of cavity modes with the OAP setup. The spectrum shows regular cavity modes with a spacing of 446 MHz.

the relation given in Equation 2, where c is the speed of light and L the length of the cavity.

$$FSR = \frac{c}{2L} \tag{2}$$

The spacing of the modes indicates a cavity length of ∼34 cm, which matches the length of the benchtop polarizer separation along the beam path.

Cavity modes have been observed in this system both when sweeping the frequency of the radiation and keeping the length of the cavity constant (see Figure 4) and when dithering the length of the cavity at a given frequency (see Figure 5). Figure 4 displays several non-TEM_{00} modes, indicating that the cavity was not well aligned and some off-axis modes were illuminated. The results shown in Figure 5 indicate a better aligned cavity resulting in only on-axis, TEM_{00} modes, but a significant baseline drift is observed between the modes. This drift arises from the detector electronics, and is addressed in more detail in Section 2.1.3. Analysis of the widths of the modes

achieved with this setup (best $\Delta\nu = 1.7$ MHz) indicates a best-case scenario of R = 98.8% for the effective cavity reflectivity according to Equation 3.

$$\frac{FSR}{\Delta\nu} = \frac{\pi\sqrt{R}}{1-R} \tag{3}$$

This effective reflectivity is limited by a number of factors, many of which will be addressed in subsequent sections. Perhaps most importantly, the effectiveness of the polarizers to serve as reflectors depends on the polarization of the light interacting with them. As a result, any optical component or process which alters the polarization of that light from the required orientation for reflective interaction with the polarizers will affect the ultimate achievable reflectivity. Further, the polarizers themselves have a degree of inherent loss due to both manufacturing defects and the physical properties of the metal grids themselves [13]. The former is a result of using polarizers which are on loan or were acquired from a rejected stock slated for use in the Herschel Space Telescope. While the known defects should still allow for sufficient operation for proof-of-concept work, defect-free models will be acquired for actual spectroscopic studies. The latter can be controlled by purchasing polarizers made from metal which provides sufficient reflectivity such that it is not the dominate loss factor (this is already the case in the current setup). Finally, the properties of the radiation beam itself can be a source of loss, as misalignment or an improperly controlled beam shape can cause light to escape the cavity prematurely.

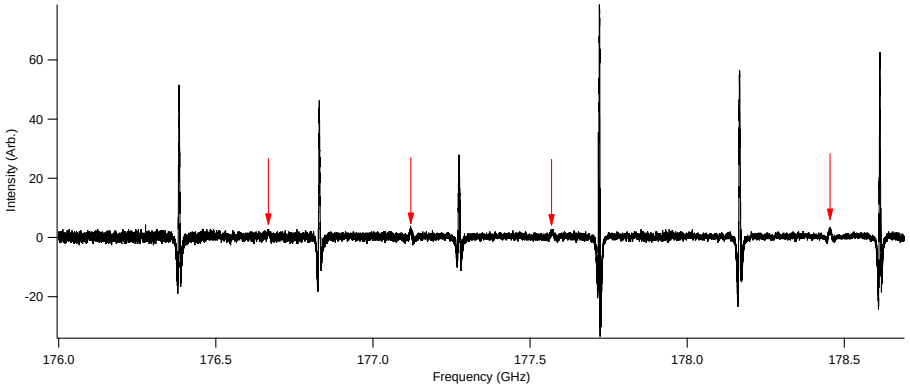

Figure 4: Second-harmonic detection of cavity modes obtained by sweeping the frequency for a cavity of constant length. Several non-TEM_{00} modes of weak intensity can be observed in the spectrum as indicated by the red arrows.

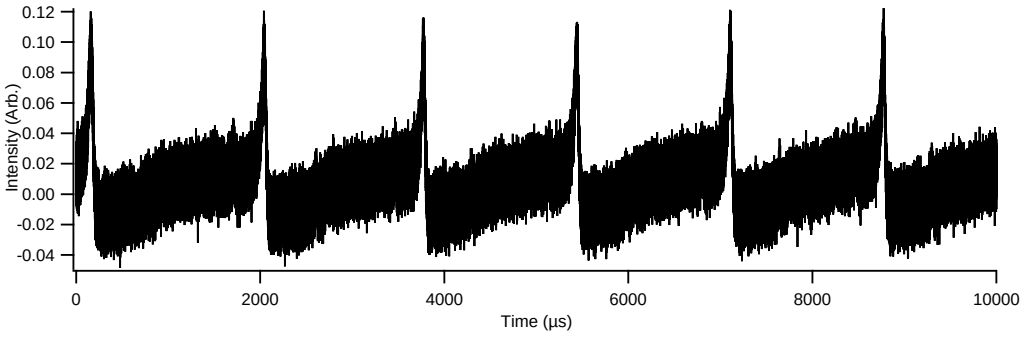

Figure 5: Cavity modes detected by dithering the length of the cavity with the translation stage, keeping the frequency constant, and recording the intensity as a function of time. The baseline between modes shows significant intensity drift.

2.1.2 Interaction of Polarized Light With System Components

The main priority of all subsequent cavity tests has been to increase the reflectivity of the cavity and/or the time constant of the cavity such that a ringdown signal could be acquired in benchtop tests. The highly-reflective nature of the cavity is dependent on the assumption that the polarization of the light does not change once it reaches the first polarizer. We discovered through early cavity tests that one property of OAPs is the induction of a degree of cross-polarization of light, where some portion of the light hitting the OAP is rotated 90°. As a result, any such rotation of light in the cavity would result in a net loss of cavity reflectivity. This is not an issue when the degree of cross-polarization is much less than the systematic losses in the cavity.

The fraction of the power reflected into the cross-polarized component is given by Equation 4, where w_m = beam waist, f = focal length, and θ_1 = OAP angle [14].

$$K_{co} = 1 - \frac{w_m^2}{4f^2} tan^2\theta_1 \tag{4}$$

Using the specifications for the 90° OAP initially used (see Table 1), it was determined that an unacceptable degree of cross-polarization ($\sim 6\%$) was occurring, drastically reducing the effective reflectivity of the cavity. As a result, a 15° OAP with an aluminum reflective surface was obtained that has a cross-polarization of roughly two orders of magnitude less than the current achievable reflectivity of the cavity. In addition, the low-angle nature of this OAP allows the cavity to be much more spatially compact, which will greatly simplify the optical setup required when the system is ultimately incorporated into a vacuum chamber.

Further concerns have arisen concerning the possibility of the polarizers themselves rotating the polarization of the light, resulting in similar loss issues to that of the cross-polarization losses caused by the OAP. To test this, the cavity was removed

Table 1: OAP specifications for the first, 90° OAP, and final 15° OAP

Spec	15° OAP	90° OAP
f	516.81	101.6
w_m	50.8	50.8
θ_1	15	90
Cross Pol	0.9998	0.9375

from the setup and the tungsten and gold polarizers were placed in the beam path immediately after the mode-matching optics. The polarizers were separated by ∼9 cm. A 10 cm focusing lens was placed immediately after the polarizers, followed by the bolometer for detection. Several tests were performed to determine how the polarizers functioned both individually and as a set with respect to the total signal detected given a variety of polarizer orientations. The results of these tests are summarized in Figure 6 and described in detail here.

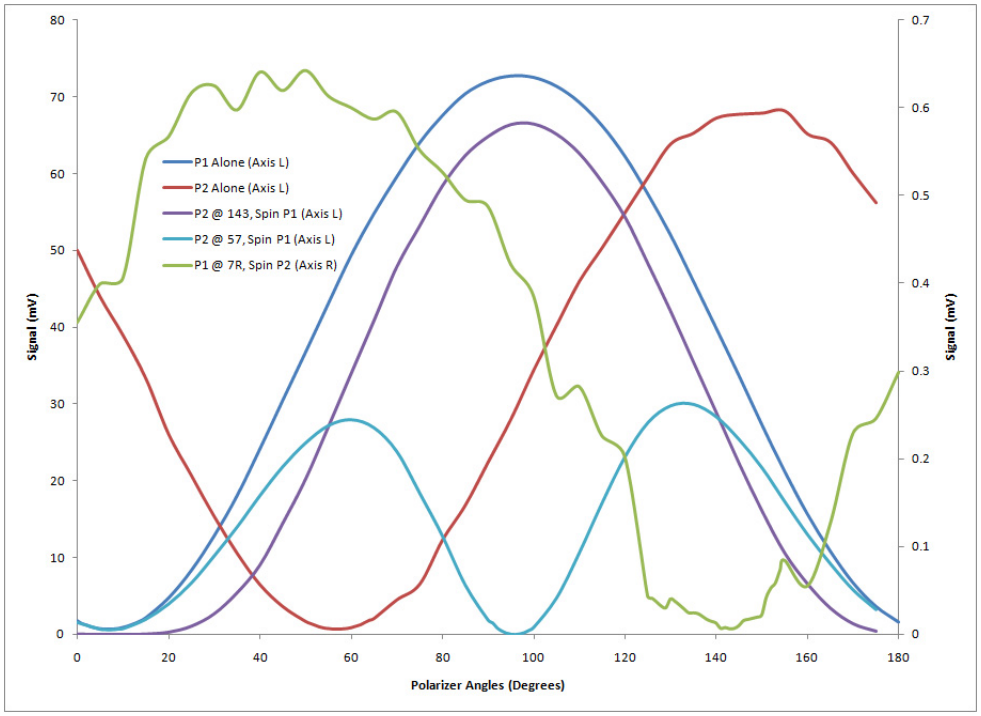

Figure 6: Detected signal through one or both polarizers in a variety of configurations over 180° of rotation.

For these tests, the tungsten polarizer was closest to the multiplier and is designated "P1," while the gold polarizer was closest to the detector and is designated

"P2." In each test, the polarizers were rotated in 5° increments over 180° of rotation, except near extrema, where 1° increments were used to show detail. To begin, each polarizer was placed into the system in its designated position without the other polarizer present and rotated through the set of angles. The results are shown in the blue and red traces, and display the expected behavior: one point of maximum transmission and one point of maximum reflectivity through 180° of rotation.

Next, both polarizers were placed in the system and P2 was set to 143°, corresponding to the orientation for maximum transmission. P1 was then rotated through the set of angles. This trace is shown in purple and displays the expected behavior as well, closely mimicking the individual trace from this polarizer (shown in blue) but with slightly less power, most likely due to losses from P2.

Next, P1 was set for maximum reflectivity and P2 was rotated through the set of angles. This is shown in the green trace and on the right axis, with normal behavior displayed and the signal intensity always being less than or about equal to the transmission through P1 at maximum reflectivity, as is expected.

Finally, P2 was set for maximum reflectivity and P1 was rotated through the set of angles. This trace is shown in light blue, and displays very unexpected behavior. The polarizer exhibited a double peaked curve, with two areas of maximum transmission and two of maximum reflectivity. Further, although P2 was set for maximum reflectivity, the detectable signal was increased substantially over the baseline of P2 by itself with the addition of P1 to the system. The cause for this behavior is still unknown. Current setups use the configuration that produces the minimum shown in the green trace (P1 at maximum reflectivity for the polarizer alone, with P2 set at 143°) as this displays both the expected behavior the the maximum observed reflectivity.

2.1.3 Current Status and Latest Results

The most recent bench-top setup for this system is shown in Figure 7. A microwave synthesizer outputs radiation from 1-50 GHz, which is passed through a Virginia Diodes multiplier system and provides tuneable free-space radiation from 50 GHz - 1.2 THz. This radiation is passed through mode-matching optics, which roughly collimate the beam before it passes through the first polarizer and enters the cavity. The cavity is currently formed by one tungsten polarizer, a 15° aluminum OAP, and a gold polarizer. The gold polarizer is placed a distance away from the OAP equal to the focal length of the OAP and at an angle perpendicular to the incoming radiation. The polarizer is mounted on a movable translation stage so that the length of the cavity can be easily altered. The radiation that leaks out the back of the second polarizer with each pass is focused through a lens onto a helium-cooled InSb hot electron bolometer and the signal is monitored on an oscilloscope and/or digitized and sent to a computer for analysis.

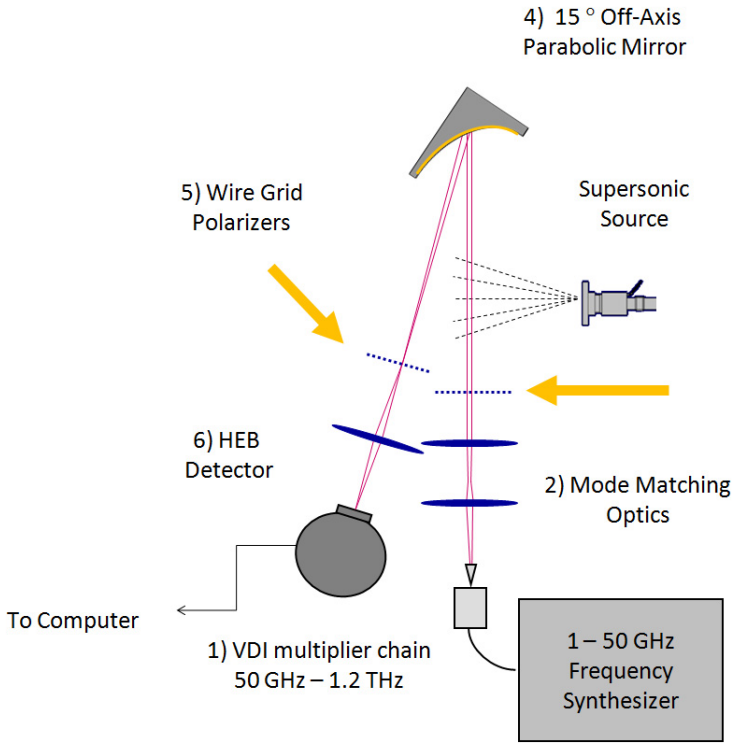

Figure 7: Current benchtop THz-CRDS setup.

Using custom code written by former group member Mr. Brandon Carroll, a threshold intensity can be selected, and the input radiation shut off once this threshold is reached so that the decay signal out of the cavity can be monitored. Analysis of initial attempts to detect a cavity build-up event and subsequent ringdown revealed a problem in the function of the detector. The AC pre-amplifier installed with the detector has an auto-leveling circuit which, on relatively short time scales, adjusts its output voltage to zero given a constant input signal. This can be clearly seen in Figure 5, where the signal shows a consistent drift in time between each cavity mode. While this not an issue for direct absorption spectroscopy, where the input signal is modulated much faster than the detector's leveling time, it presents a significant hurdle to accurately monitoring and modeling ringdown events, which occur on much longer time scales than this drift and cannot be easily modulated. A DC pre-amplifier which does not auto-level was constructed by the manufacturer and has recently been installed, eliminating this problem. Subsequent tests should focus on tuning the cavity to produce a single, measurable build-up event, followed by a measurable decay signal on the benchtop before integration of the system with the vacuum chamber for full spectroscopic operation. This is discussed more fully in Section 4.

2.2 Spectroscopy of Transient Species

In addition to increasing spectral sensitivity for the study of radicals and ions, appropriate production techniques for these molecules must also be developed. To this end, I have designed four pulsed, supersonic expansion sources coupled with a variety of configurations of electrical discharges. Two of these sources are based on the well-proven source designs of McCarthy and Thaddeus described in reference [16]. The versions of these sources designed for the protonated methanol experiment are shown in Figure 8. Here, the pulsed valve is kept at earth ground through its connection to the vacuum chamber, while the outer electrode is attach to negative high voltage,

typically ∼1000 V. A plasma discharge then occurs between the electrode and the pulsed valve whenever gas is present in the channel. The "compact" McCarthy-style source (Figure 8a) has been used for all work presented here. This source has several advantages that lend themselves to early testing and benchmarking. First, the source requires only two custom-machined components (the teflon cap and ring electrode), which aids in both simple setup and consistent reproduction. Second, this source has fewer degrees of freedom than other sources in terms of number of electrodes, machined-spacers, and untested, complex parts.

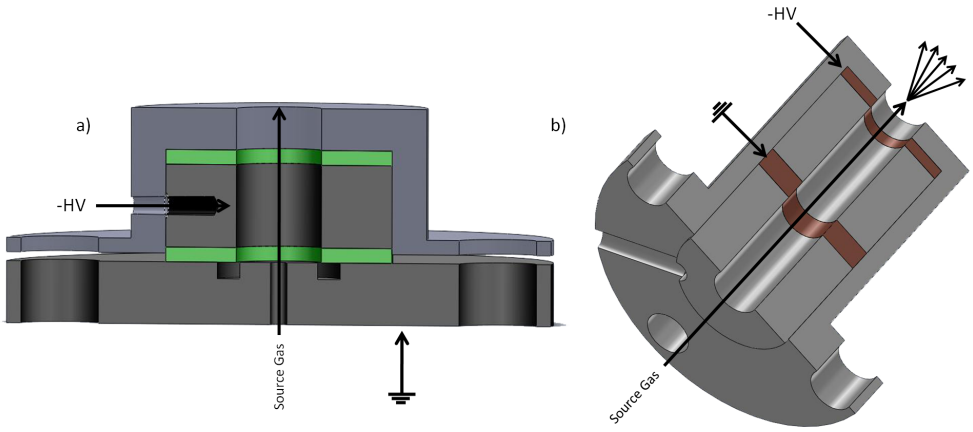

Figure 8: a) Compact McCarthy-style source b) Traditional McCarthy-style source.

In the case of the traditional source (Figure 8b), a bias can be applied to the inner electrode to alter the conditions of the discharge to increase production efficiency depending on the nature of the target molecules (e.g. anions, cations, radicals, etc.). The other two sources, both of which are loosely based on attempts by Amano and coworkers to incorporate a hollow cathode discharge into a supersonic expansion source [17, 18], are shown in Figures 9 and 10. The first is constructed using the "compact" McCarthy-style source with a metal sphere attached at the base and extending out past the throat of the expansion to serve as the cathode. The discharge occurs after the molecules have expanded, with the plasma forming within the sphere and exiting out the front into the chamber. This design raises some concerns. First,

the expansion region is shortened for post-discharge-cooling which will most likely result in hotter molecules than the McCarthy-style sources. Also, the large distance from the throat of the expansion to the region that can be probed with the radiation may limit the obtainable signal-to-noise ratio, as the expansion density will be low at this distance.

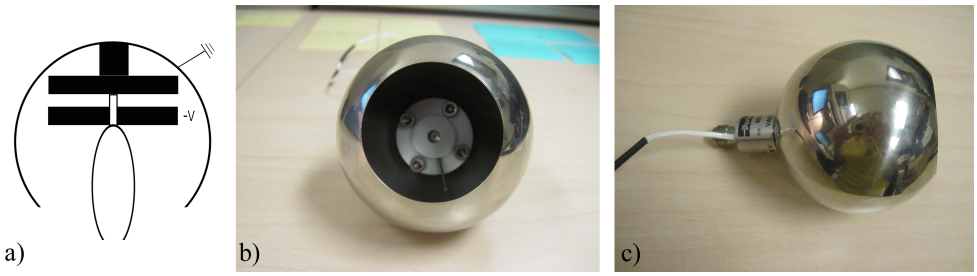

Figure 9: a) Cutaway diagram of a source constructed with the discharge occurring post-expansion, b, c) pictures of the source from a face-on and side perspective.

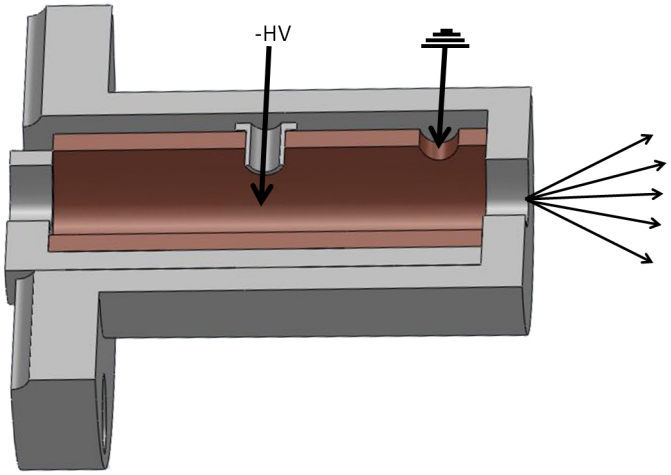

Figure 10: Novel source for integrating a hollow cathode source prior to the expansion.

To address these issues, I designed a novel source which incorporates a cylindrical cathode prior to the expansion into the chamber (see Fig 10). A small metal wire, fed into the cathode through a teflon sheath inserted into a through-hole in the center of the cathode, serves as the anode. This source will allow for ample cooling

post-discharge and the ability to align the probe beam very close to the throat of the expansion. For utility, this source is designed to use the same teflon cap as the McCarthy-style source, with a simple slit cut down the side to allow access to the cathode and anode for the ground and high voltage wires.

While the CRDS system required for the detection of protonated methanol is under development, experiments were constructed to test the ionization abilities of the sources using a simpler chemical system, the collisional complex H_5^+. The sources are also capable of producing high-energy neutral species, which may be easier to detect than ions. Astronomical investigation of the high-energy neutral species *trans*-methyl formate would also greatly benefit from measurement of transitions in the millimeter and submillimeter frequency ranges. Initial spectroscopic studies therefore also targeted this molecule. For these studies, the simple direct-absorption spectrometer shown in Figure 11 was constructed. The chemical motivations for studying each of these species is overviewed below, and results from preliminary experiments to investigate their spectra are reported.

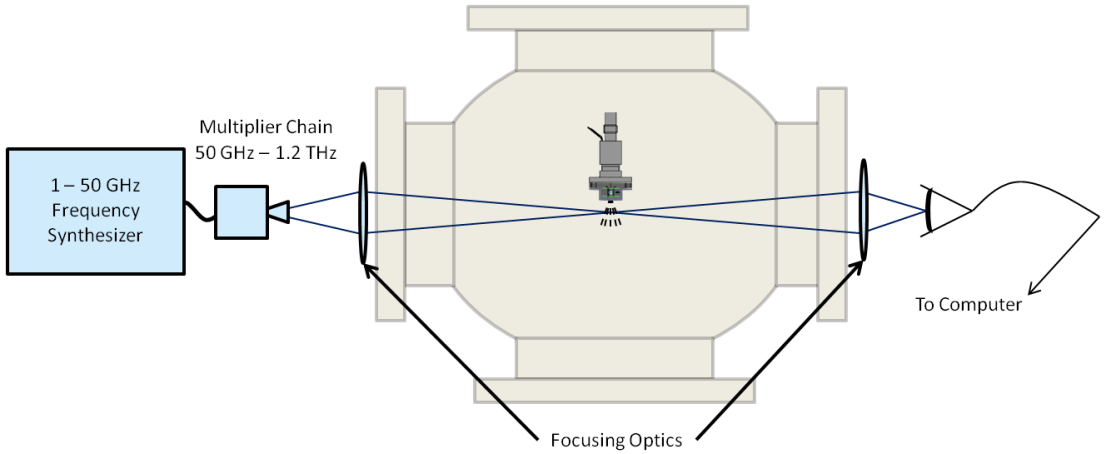

Figure 11: Basic schematic of direct absorption spectroscopy setup.

2.2.1 H_5^+

Hydrogen is the most abundant element in the universe, and as such greatly affects the chemistry occurring in the ISM. H_3^+, the simplest polyatomic molecule, is a major constituent in hydrogenic plasmas and in interstellar environments. The reaction of H_3^+ with H_2 is the arguably most common bimolecular reaction in the universe and greatly influences the properties of H_3^+ and the extensive chemistry that results from its reactions with more complex molecules. This reaction proceeds through the H_5^+ complex:

$H_3^+ + H_2 \rightarrow H_5^+ \rightarrow H_3^+ + H_2$

The detection of H_5^+ in astronomical environments and in terrestrial atmospheric and combustion chemistry, would provide invaluable insights into the role of this most fundamental reaction.

The electronic structure and potential energy surface of H_5^+ has been extensively studied, with the most complete and accurate determination being that of Xie et al. [23]. Using the structure obtained for the ground state, equilibrium, global-minimum geometry, the rotational constants A, B, and C were calculated and a spectrum predicted using the PGOPHER program [24]. The fundamental transition (1_{11}-0_{00}) is predicted to fall at 901504 MHz, and this transition was selected for a targeted search.

Hydrogen was fed directly into the discharge source with a backing pressure of 12 psi, resulting in a sample pressure of ∼90 mTorr. The discharge was operated at ∼1 kV. Due to the highly fluxional nature of the H_5^+ complex, and because the constants generated from the structure did not include zero-point energy corrections or torsional splittings, the predicted frequency for the transition was taken only as a rough starting point. Scans were taken on either side of the predicted frequency in 200 MHz increments, with the majority of scans being averaged 5 times. The resulting spectrum is shown in Figure 12 and clearly shows a lack of any spectral features.

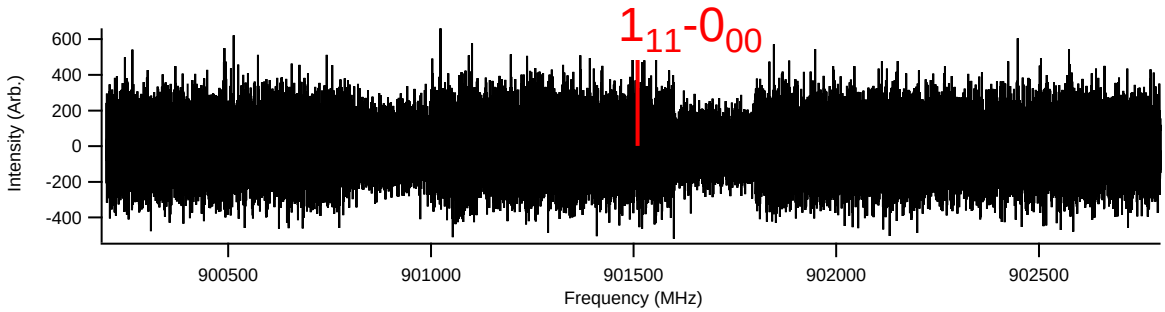

Figure 12: 900.2 - 902.8 GHz scan of H_2 discharge, with the predicted fundamental transition frequency shown in red.

This clear non-detection lead to a reexamination of the structural properties of H_5^+. While the ground-state, equilibrium geometry is indeed a C_{2v} structure as described in Xie et al. [23], the structure changes significantly when zero-point energy contributions are taken into consideration. In fact, the ground state, zero-point averaged structure is of a completely symmetric D_{2d} geometry, with no permanent dipole moment [25]. Thus, H_5^+ does not have a pure rotational spectrum. An analysis of the effects of deuteration on the symmetry of the complex followed from this initial examination of the main isotopologue.

The results of this analysis have been recently published [26]. When zero-point energy is taken into account, H_5^+, D_5^+, and HD_4^+ all display completely symmetric structures (with the proton shared equally between the two D_2 moieties in the case of HD_4^+), while H_4D^+, $H_3D_2^+$, and $H_2D_3^+$ all have at least one non-zero dipole-moment component (see Table 2).

Table 2: Rotational constants and dipole moments for H_5^+, H_4D^+, $H_3D_2^+$, $H_2D_3^+$, HD_4^+, and D_5^+. [26]

Species	A (GHz)	B (GHz)	C (GHz)	μ_a (D)	μ_b (D)	μ_c (D)
H_5^+	748.0	92.0	92.0	0.00	0.00	0.00
H_4D^+	641.3	77.0	75.5	0.12	-0.04	0.00
$H_3D_2^+$	503.7	69.6	66.6	-0.20	0.00	0.00
$H_2D_3^+$	456.0	54.9	53.7	-0.09	0.00	-0.04
HD_4^+	381.9	48.0	48.0	0.00	0.00	0.00
D_5^+	381.9	47.1	47.1	0.00	0.00	0.00

The dipole moments and rotational constants determined in this work where then used to simulate pure-rotational spectra for H_4D^+, $H_3D_2^+$, and $H_2D_3^+$ up to 3 THz at both 20 K and 300 K using a standard asymmetric top hamiltonian and the CALPGM suite of programs [27]. These spectra are shown in Figure 13 which is reproduced from Figure 2 of reference [26].

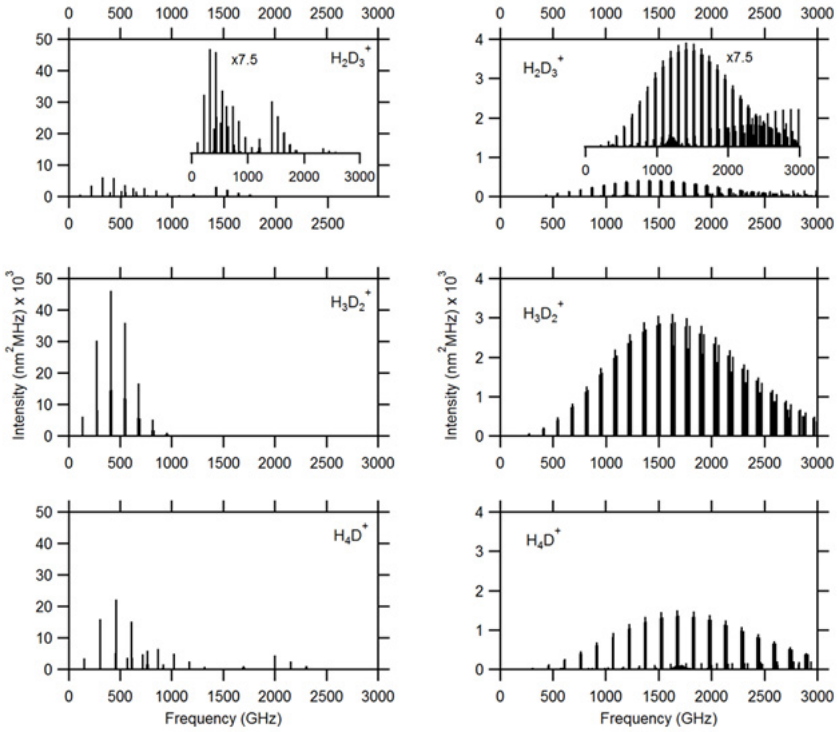

Figure 13: Simulated pure rotational spectra at 20 K (left) and 300 K (right) for H_4D^+, $H_3D_2^+$, and $H_2D_3^+$. [26]

These spectral predictions are intended for use as a rough guide for laboratory spectroscopic searches for these molecules. H_5^+ and its isotopologues are highly fluxional species, with low barriers to internal rotation of the H_2, HD, and D_2 moieties ($\sim$ 160 cm^{-1} [23, 25]) and low lying excited torsional bands (likely to fall between those calculated for H_5^+ and D_5^+ of $\sim$ 80 and $\sim$ 32 cm^{-1}, respectively [25]. As a result of these factors, significant spectral complexity is expected beyond the predictions shown in Figure 13. The spectra are expected to display multiplet splitting due to the internal rotation, and also experience significant perturbation due to torsion-rotation

coupling, especially in the 1 - 2.5 THz range, where the energy match between the pure-rotational and excited torsional state transitions is greatest. Nevertheless, the predictions should serve as excellent guides for the best regions within which to begin searches for spectral lines arising from these molecules. Ongoing efforts to obtain spectra of these isotopologues are expanded upon in Section 4.

2.2.2 *Trans*-Methyl Formate

The discharge sources described in section 2.2 are also capable of producing high-energy neutral species. Methyl formate exists in both a *cis* and *trans* conformation, with the *trans* conformer lying ∼2000 cm^{-1} above the *cis* conformer. The barrier to isomerism between these conformers is ∼5000 cm^{-1} and at room temperature, the population ratio is ∼30,000:1 *cis*:*trans*. Laboratory experiments in the Pate group using a supersonic discharge source for production of *trans*-methyl formate showed a 50:1 population ratio [19]. Recent astrochemical models have predicted a ratio on the order of 10:1 *cis*:*trans* at long timescales in interstellar clouds [20]. Although a tentative detection of the *trans* species has been made using the Green Bank Telescope based on several experimentally measured, low-frequency transitions [21], confirmation of this detection, and an accurate determination of the interstellar abundance, relies upon the laboratory measurement of higher-frequency transitions of the *trans* species.

Initial alignment of the system and optimization of experimental parameters was performed using methanol, a neutral species with strong, experimentally measured transitions. A spectrum of methanol from 193.440 - 193.513 GHz showed 12 transitions (see Figure 14). A semi-quantitative Boltzmann analysis of the transitions conducted by comparing the relative line intensities indicated a methanol rotational temperature of 20-40 K in the expansion.

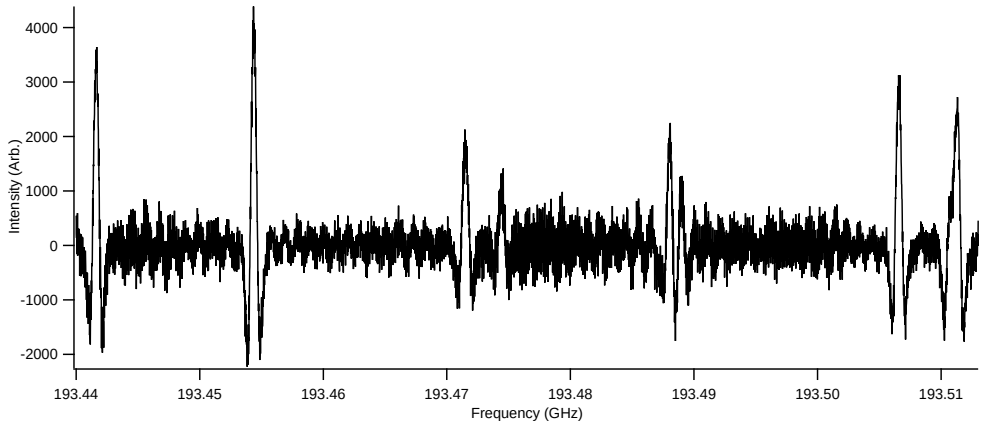

Figure 14: Spectrum of methanol showing rotational temperatures between 20-40 K. Etalon effects arising from the two plexiglass flanges surrounding the vacuum chamber are clearly visible.

Methyl formate was introduced into the system by bubbling argon through a reservoir of room temperature liquid methyl formate and subsequent mixing with argon gas. The relative concentrations of methyl formate vapor and argon were adjusted incrementally until *cis*-methyl formate lines were observed (see Figure 15).

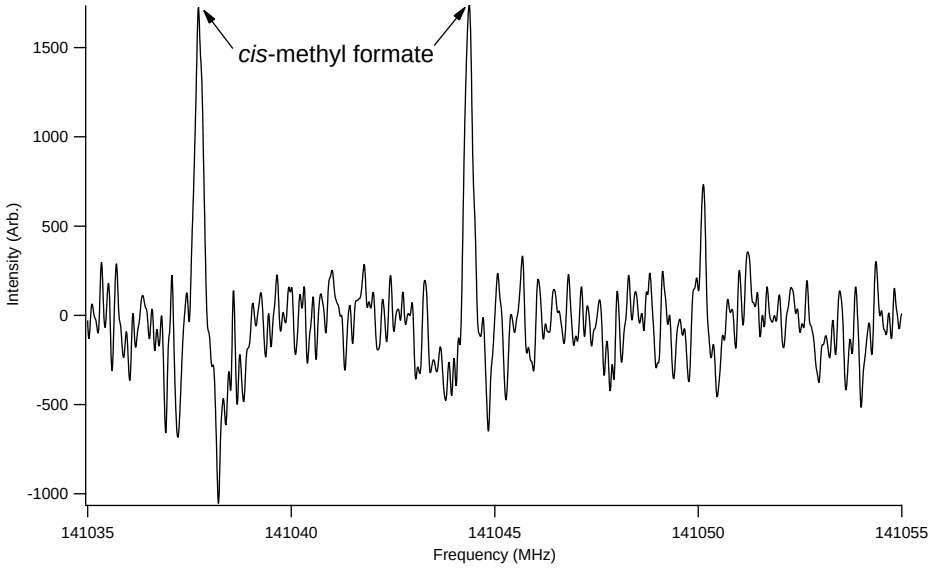

Figure 15: Smoothed spectrum of *cis*-methyl formate $12_{2,11}$-$12_{2,10}$ A & E transitions. The third line at 141050 MHz has not been identified.

A number of lines were observed after 10 averages during the first scan with the discharge on (see Figure 16). As can be seen in Figure 16, these lines are clearly

present with the discharge both on and off. Further, only one *trans*-methyl formate line is predicted in this frequency range based on publicly available molecular line catalogs. There are no matches to measured or predicted lines at these frequencies in either the Jet Propulsion Laboratory (JPL) [22] or Cologne Database for Molecular Spectroscopy (CDMS) [1] databases. This leaves the origin of the observed lines in question.

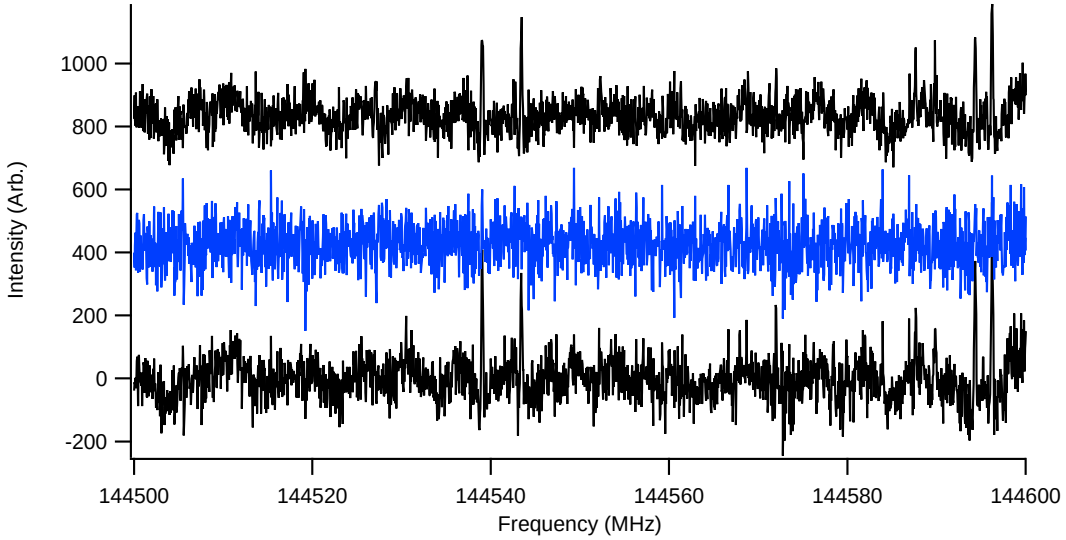

Figure 16: Spectra taken with both the discharge on (bottom) an off (top, with a y-offset). A difference spectrum is shown in blue (with a y-offset). There are no lines present with the discharge on that are not also present with it off.

Further studies showed a large number of lines in almost every frequency region observed. All of these lines are present with the discharge both on and off, indicating that they are almost certainly not due to *trans*-methyl formate. A handful can be attributed to previously observed and assigned *cis*-methyl formate transitions. The methyl formate sample used in this study also contains ∼3% methanol, and a small number of the lines can be further attributed to known methanol transitions. The total number of observed lines identifiable as *cis*-methyl formate or methanol, however, is quite small. It is possible the remaining lines are unassigned transitions of *cis*-methyl formate, as the spectrum of this molecule is quite complex. Methyl formate

is also a good organic solvent, so it is possible that the sample is contaminated with impurities from the plastic tubing used to deliver the gas to the chamber.

As in the H_5^+ experiment, given the weak spectral intensity of *trans*-methyl formate, the short pathlength, the limited sensitivity, and uncertainties in the predicted frequencies, it is not surprising that *trans*-methyl formate was not detected. These searches are ongoing and several possibilities for improving the chances of detection are discussed in Section 4.

3 Astronomical Observations

A major goal of this work is to provide the high-resolution spectra of complex chemical species required for definitive astronomical detections that help to further our understanding of the physical and chemical processes at work in the ISM. Of the nearly 160 molecules which have been detected in the interstellar medium (ISM), a large fraction are complex organic molecules (COMs) - those organic species containing five or more atoms [28]. Recent theoretical [29] and laboratory [30] studies have shown that textbook gas-phase reaction pathways (e.g. ion-molecule and electron recombination reactions) are not efficient processes for the production of COMs. Instead, the formation of these molecules is now thought to be dominated by chemical reactions occurring on the icy surfaces of dust grains [31], with the most recent models predicting that radical-radical reactions induced by photolysis processes play a significant role [32]. The products of the grain surface chemistry are then liberated into the gas phase via evaporative processes or shocks after their production.

Although current gas-grain astrochemical models incorporate nearly 740 species and over 7800 reactions, both in the gas phase and on grain surfaces, their refinement is limited by the availability of observational data with which to constrain the chemistry. Due to its rich chemical inventory [33], the hot core Sagittarius B2(N) has been the primary focus for comparison to models. It is difficult to claim that

this source is typical of interstellar chemical inventories and physical conditions, as it has been shown to have the richest chemistry of any source observed to date [33]. It is therefore desirable to obtain complete molecular inventories of a wider variety of these types of sources to use in refinement of models of chemical evolution in the ISM. In contrast to targeted searches, such surveys provide not only a more complete picture of the chemical inventory of the source, but allow for more accurate determination of the physical conditions in which these molecules exist. Further, having these broadband spectra in-hand allows for rapid identification of new species in the observed sources when experimentally determined transitions for a molecule become available in the laboratory. To this end, I have conducted broadband spectral line surveys of two interstellar environments known to contain COMs. These surveys are part of our ongoing, larger effort to conduct such studies on a variety of sources and environments in the ISM with the aim of refining astrochemical models and guiding laboratory studies on species of interest.

3.1 G+0.693-0.027

The central molecular zone (CMZ) of the GC is known to be less dense and have far lower excitation temperatures (∼10-20 K) and dust temperatures (∼20 K) than those found in star-forming regions containing hot cores and hot corinos [34]. Yet, recent work has shown that while the absolute abundances of COMs varies greatly not only between these types of sources but within various targets of the same type, the relative abundances of COMs are almost constant between sources [35]. Given the widely varying conditions of temperature and density in the gas phase between these types of sources, the similar abundances suggest the formation of these COMs on grain surfaces. Here, the inherent differences in initial ice composition can account for the variety of absolute abundances between sources and yet also account for the similar relative abundances between different source types. Additionally, the

low-temperature nature of these sources results in decreased molecular partition functions. This in turn shifts population in rotational (and vibrational) energy levels to heavily favor the lower-energy states, with populations directly related to the Boltzmann distribution associated with that temperature. As a consequence, the spectral complexity is greatly reduced as transitions arising from (or going to) higher-energy states will be far less intense (often below detection threshold) and transitions arising from the highly populated lower-energy states will be more intense, favoring easier detection. This allows for easier spectral line assignment and determination of physical parameters. These regions in the GC therefore represent ideal sources for observational studies that sample the full chemical inventory and range of physical conditions. This information can then be used to constrain the chemical models that incorporate COM chemistry.

To this end, have we obtained deep spectral integrations for five sources in the GC known to contain methyl formate ($HCOOCH_3$). Methyl formate is a COM known to be produced efficiently only via grain-surface reactions [29] and is therefore widely considered as an excellent tracer of complex interstellar organic chemistry. After obtaining the preliminary deep integrations for each of the five sources, the source that showed the greatest number of strong spectral lines associated with COMs in the selected frequency range was chosen for an unbiased, broadband spectral line survey.

3.1.1 Observations and Data Reduction

The observations were conducted over a five night period in mid-July, 2010, using the Caltech Submillimeter Observatory on Maunea Kea, Hawaii. The double side band (DSB) receiver was tuned to a variety of LO frequencies which were in turn sampled over a range of IFs to obtain complete coverage for deconvolution of the spectrum. Values of T_{sys} varied widely from night to night, ranging from 271 to 695

K, and requiring integration times between 2.3 and 16 minutes, respectively, to reach an expected RMS of 30 mK.

Deep spectral snapshots were obtained over the frequency range of 236.45 - 240.56 GHz (rest) and 249.55 - 251.46 GHz (image) towards five sources in the GC (see Table 3). The frequency range was selected for the variety of COMs and other molecules with transitions in these frequency windows [36]. The convolved, DSB spectra are shown in Figure 17. Each spectrum was integrated to obtain an expected RMS of 30 mK. G+0.693-0.027 was selected for the broadband survey due to the molecular complexity and high spectral intensity relative to its counterparts.

Table 3: Targeted Galactic Center Sources

Source	RA	Dec
GCM -0.11-0.08	17:45:39.12	-29:04:04.8
GCM -0.08-0.06	17:45:41.04	-29:02:13.2
GCM +0.24+0.01	17:46:10.08	-28:43:40.8
GCM +0.694-0.017	17:47:09.77	-28:21:07.9
GCM +0.693-0.027	17:47:21.86	-28:21:27.0

The CLASS software package included in the GILDAS suite of programs [37] was used for cleaning and deconvolution of the spectra. Baselines were removed from each scan either by fitting a first degree polynomial function to the baseline, or by applying an empirically-determined constant offset when line density prohibited a reliable baseline fit. The spectrometers used to acquire the spectra introduced a number of large-amplitude noise spikes into the data. These were easily identified and removed due to their substantially different profiles and intensities relative to spectral features. The spectra were then resampled to a channel spacing of 0.749 MHz.

The standard deconvolution routine included in the CLASS distribution was used to convert the double-sideband spectra to one signal-averaged single-sideband spectrum assuming no gain variations between the upper and lower sidebands. This solution was then used as the initial guess for a second deconvolution allowing gains

Figure 17: Spectral snapshots of the five GC sources listed in Table 3

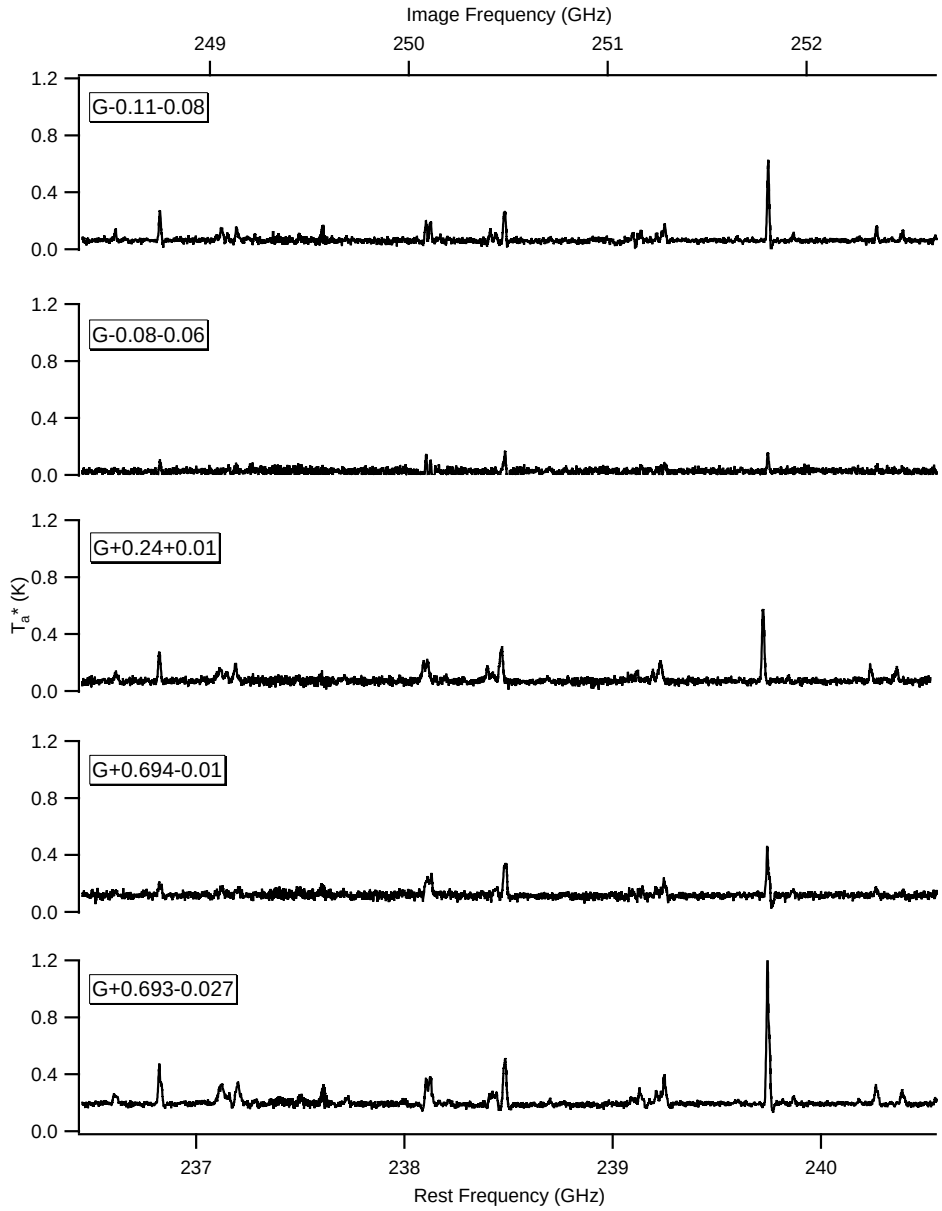

to vary. Due to the nature of the routine being used, very strong lines (relative to the rest of the spectra) can cause ghost images to appear in the final deconvolution. To avoid this complication, a second set of deconvolutions were performed with several frequency ranges masked to remove these strong lines from the spectrum during the deconvolution process. The lines were then stitched back into the final spectrum using

the average center frequencies and intensities from the initial set of deconvolutions. The frequency ranges masked in this case are given in Table 4.

Table 4: Frequency ranges masked during the deconvolution of G+0.693-0.027.

Species	Transition	Lower Limit (MHz)	Upper Limit (MHz)
^{13}CO	J $(2 \rightarrow 1)$	220254	220516
C_2H_5CN	J_{K_a,K_c} $(25_{2,23} \rightarrow 24_{2,22})$	228466	228556
CO	J $(2 \rightarrow 1)$	230428	230694
OCS	J $(19 \rightarrow 18)$	231048	231210
CH_3OH	J $(5 \rightarrow 4)$ Branch	241668	241937
CH_3OH	$J^p_{K_a}$ $(5^-_1 \rightarrow 4^-_1)$	243888	243947
CS	J $(5 \rightarrow 4)$	244896	244893

The resulting deconvolved spectrum is shown in Figure 18. Sufficient coverage was available to allow full deconvolution from 219345 to 251008 MHz with a 1 GHz gap at 230561 MHz. Of the major COMs targeted in our studies (methanol, acetamide, dimethyl ether, ethanol, ethyl cyanide, formaldehyde, formic acid, glycolaldehyde, methyl cyanide, and methyl formate) only methanol, ethanol, and formaldehyde can be definitively identified in the spectra. Dimethyl ether is likely visible as well, but only barely above the noise level. Given that the key target for this search was methyl formate, and that it has been previously detected in this source, the current observations do not reach a sufficiently high level of sensitivity. This is likely due to the fact that a large number of the DSB spectra were unreliable, mostly due to molecular line signals in the off-position used during the chopping calibration to obtain "blank" reference data during integration. The GC region is densely packed with molecular line sources that both strongly emit and strongly absorb in this frequency range. As a result, if the off-position data were not merely continuum but contained emission or absorption features, these could be averaged into the acquired spectra. This was indeed observed, necessitating the removal of the affected scans. The remaining integrations were far fewer than required for a full deconvolution, or for achieving the desired noise level, resulting in much higher RMS in the SSB, deconvolved spectra. Additional observations are required to complete a full analysis of this source.

Figure 18: Fully deconvolved spectrum of G+0.693-0.027 from 219345 - 251008 MHz.

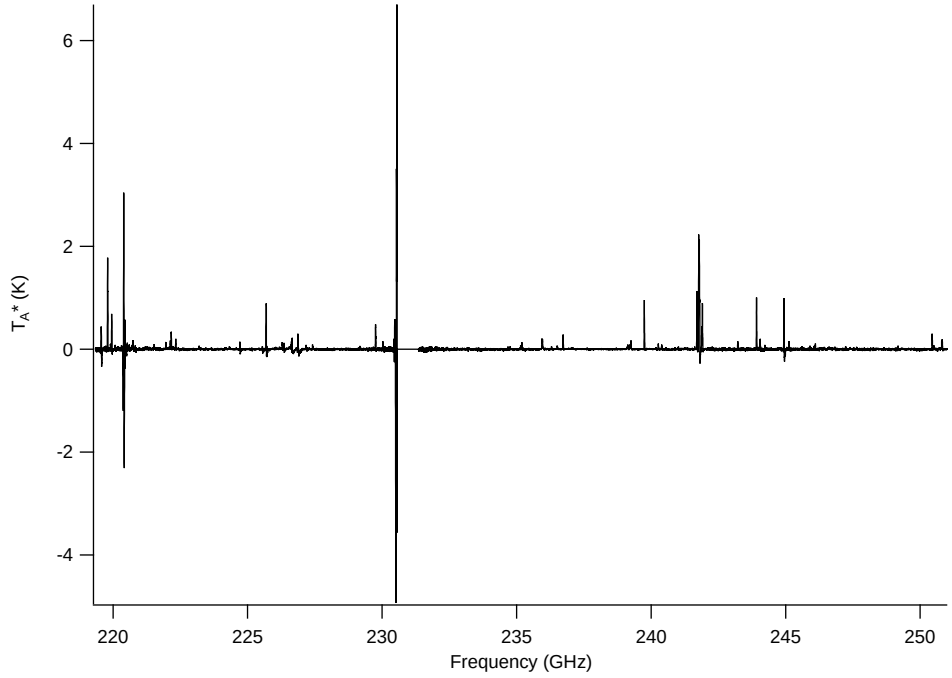

3.2 L1157

The dark cloud L1157 contains an embedded low-mass stellar object that has a bipolar molecular outflow. The source contains a number of shocked regions where the outflow interacts with the background gas. Such shocks can have a significant impact on the gas-grain chemistry of the region, as they trigger grain surface reactions and cause molecules on the grain surface to be ejected into the gas. The region we have chosen to study in detail is shown as *B1* in a map from [38] in the left panel of Figure 19. Previous studies have indicated the presence of a variety of complex organic molecules in the *B1* region, most likely formed on the grain surface before being ejected into the gas phase by the shocks [38]. Our own observations of L1157 have demonstrated the chemical richness of the *B1* region of this source. The right panel of Figure 19 shows the clear identification of SO_2, formaldehyde, and methanol, from observations obtained in 2010.

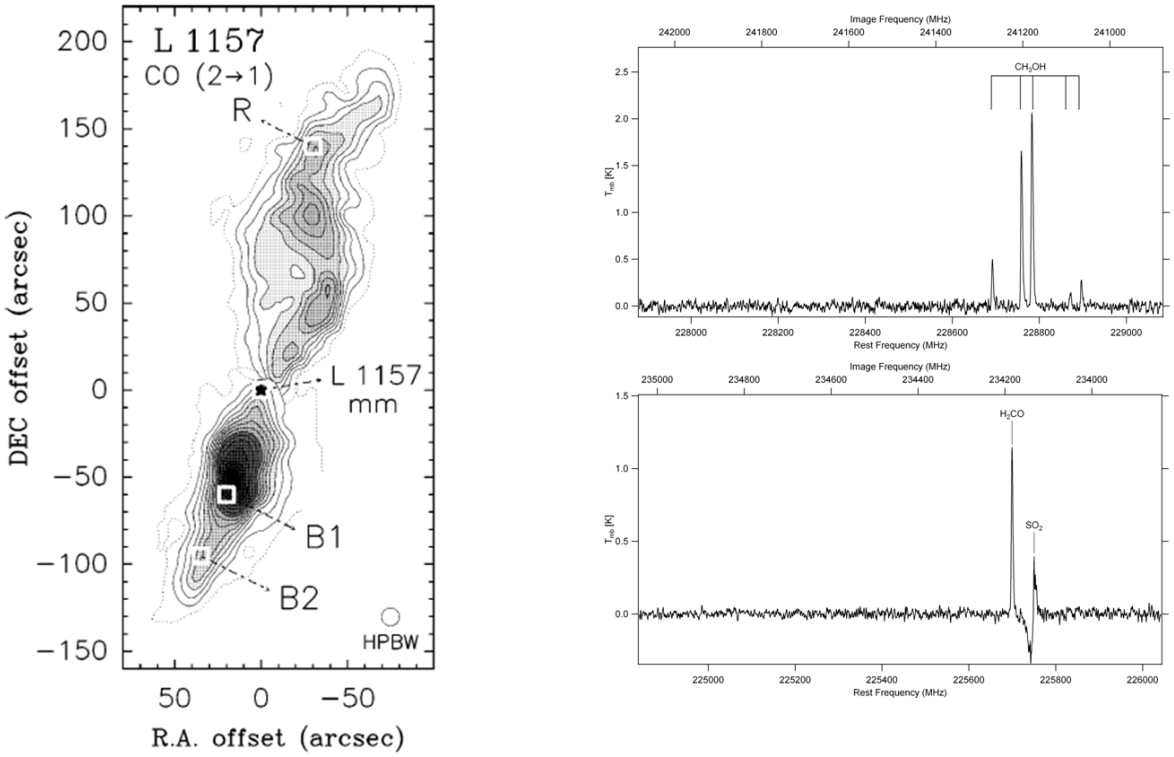

Figure 19: Left: CO 2→1 emission map of L1157. Right: Preliminary identifications of molecules from our 2010 observations.

Further observations were obtained in July 2011 that should provide sufficient coverage for a full deconvolution of these data over a ∼20 GHz range. Deconvolution and analysis of these observations are ongoing.

4 Future Work

Each of the projects described above has shown great promise, and work is underway to improve each of these experiments to enable their completion. In the laboratory, a number of improvements are planned to increase the likelihood of detection of H_5^+ and *trans*-methyl formate before moving on to study more complex species such as protonated methanol. After acquiring a ringdown with the CRDS system on the benchtop, the next step is to integrate the spectrometer into our large vacuum

chamber to begin studying species produced by the discharge sources (see Figure 20).

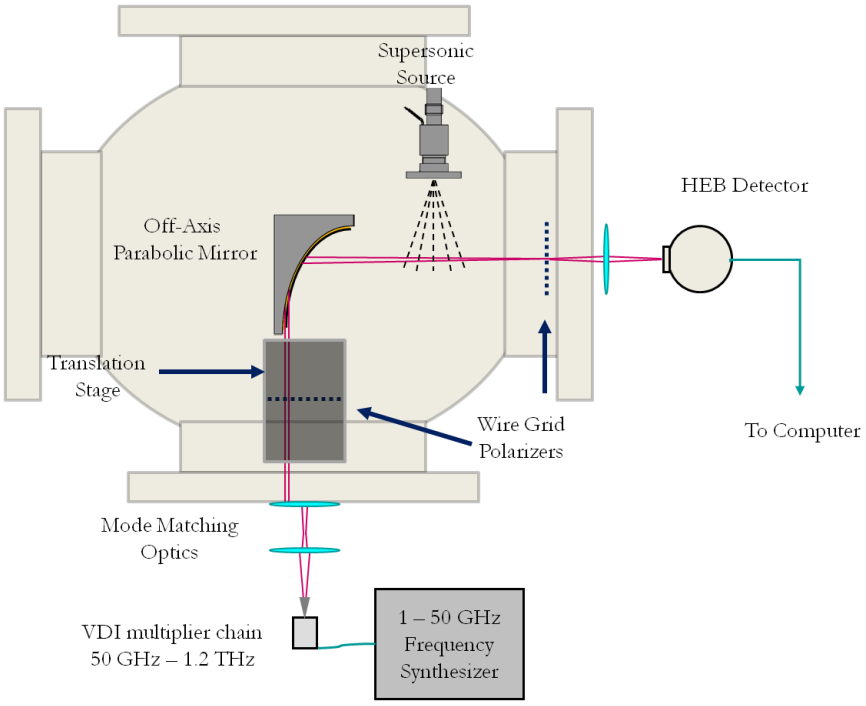

Figure 20: Planned fully-integrated THz-CRDS setup.

While the modifications to the CRDS system are underway, steps will be taken to improve the sensitivity of the direct absorption system and continue to look for transitions of *trans*-methyl formate. The focus for ion spectral acquisition will shift to the detection of the deuterated isotopologues of H_5^+ predicted to have rotational spectra. First, the pathlength of the system will be increased by splitting the gas line to the discharge source and adding two additional discharge sources operating in parallel. This should result in a factor of three increase in the observable signal.

The second improvement will involve incorporation of a new timing scheme into the discharge setup to better control the formation and cooling of target species. Specifically in the case of H_5^+ isotopologues, it has been shown that a very short high voltage pulse initiated in the middle of a longer pulse of H_2 gas dramatically increases both the production of H_5^+ and its overall cooling [39]. Even with the cooling offered by the supersonic expansion, the ions produced are relatively warm and short-lived.

By allowing them to diffuse into and collide with H_2 that was not involved in the discharge, the degree of cooling and lifetime of the ions is greatly increased.

Meanwhile, a multipass setup has been incorporated into the existing system to further increase the effective pathlength based on a cell designed by Perry and coworkers [40] (see Figure 21). This system is currently being integrated with the vacuum chamber and multiple source setup to allow for at least 20 passes through the supersonic expansion [41], which should allow for an increased spectral sensitivity roughly equal to the number of additional passes.

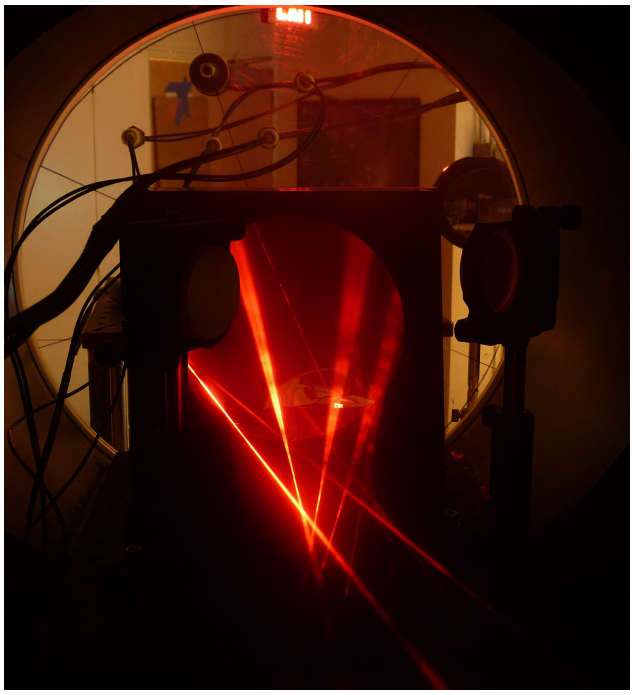

Figure 21: Perry type multipass cell integrated into vacuum chamber and traced by a HeNe laser.

Finally, the complete spectral analysis of G+0.693-0.027 will require further observations to produce a spectrum with low enough RMS to be useful for analysis of COM chemistry. After cleaning and deconvolution of the L1157 data, a local thermodynamic equilibrium (LTE) least-squares fit analysis will be performed on the spectrum to extract quantitative data on the temperatures and abundances of each of these species. These results will then be used as comparison data for future

modeling studies and also serve as catalogs for rapid identification of new molecules, such as *trans*-methyl formate and the H_5^+ isotopologues as laboratory spectra become available.

References

[1] Müller, H.S.P., Schlöder, F., Stutzki, J., and Winnewisser, G., *J. Mol. Struct.* **2005**, *742*, 215.

[2] Radhuber, M.L. et al., *Astrophys. J.* **2010**, *in preparation.*

[3] Charnley S, in The Bridge Between the Big Bang & Biology, ed. F. Giovanelli (Rome: Cons. Naz. D. Ricerche), *139*, **2001**.

[4] Droege, A.T.; Engelking, P.C., *Chem. Phys. Lett.* **1983**, *96*, 316.

[5] Engelking, P.C.,*Rev. Sci. Instrum.* **1986**, *57*, 2274.

[6] Smalley, R.E.; Wharton, L.; Levy, D.H., *J. Chem. Phys.* **1975**, *63*, 4977.

[7] Campargue, R., *J. Phys. Chem.* **1984**, *88*, 4466.

[8] White, J.U., *J. Opt. Soc. Am.* **1942**, *32*, 285.

[9] Herriott, D., Kogelnik, H., and Kompfner, R., *Appl. Opt.* **1964**, *3*, 523.

[10] O'Keefe, A. and Deacon, D.A.G., *Rev. Sci. Instrum.* **1988**, *59*, 2544.

[11] *Fundamentals of Photonics*; Saleh, B.E.A. and Teich, M.C.; John Wiley & Sons, Inc.: Hoboken, NJ, 2007, 367.

[12] Braakman, R., California Institute of Technology, *PhD Dissertation* **2009**, 96.

[13] Braakman, R. and Blake, G.A, *J. Apl. Phys.* **2011**, *109*, 063102.

[14] *Quasioptical Systems*; Goldsmith, P. F.; IEEE Press: Piscataway, NJ, 1998, 116.

[15] Romanini, D., Kachanov, A. A., Sadeghi, N., and Stoeckel, F., *Chem. Phys. Lett* **1997**, *264*, 316.

[16] McCarthy, M. C., Chen, W., Travers, M. J., and Thaddeus, P., *Astrophys. J. Suppl.* **2000**, *129*, 611.

[17] Fukushima, M. et al., *Chem. Phys. Lett.* **1994**, *230*, 561.

[18] Xu, Y., Fukushima, M., Amano, T., and McKellar, A. R. W., *Chem. Phys. Lett.* **1995**, *242*, 126.

[19] Pate, B., *Private Communication* **2010**.

[20] Laas, J. et al., *Astrophys. J.* **2011**, *728*, 71.

[21] Neill, J.L. et al., *J. Phys. Chem. A* **2011**, *115*, 6472.

[22] Pickett, H.M. et al., *J. Quant. Spectrosc. & Rad. Transfer* **1998**, *60*, 883.

[23] Xie, Z., Braams, B. J., and Bowman, J. M., *J. Chem. Phys.* **2005**, *122*, 224307.

[24] PGOPHER, a Program for Simulating Rotational Structure, C. M. Western, University of Bristol, http://pgopher.chm.bris.ac.uk

[25] Cheng, T. C., Bandyopadyay, B., Wang, Y., Carter, S., Braams, B. J., Bowman, J. M., and Duncan, M. A., *J. Phys. Chem. Lett.* **2010**, *1*, 758.

[26] McGuire, B. A., Wang, Y., Bowman, J. M., and Widicus Weaver, S. L., *J. Phys. Chem. Lett.* **2011**, *2*, 1405.

[27] Picket, H. M., *J. Mol. Spec.* **1991**, *148*, 371.

[28] Herbst, E. and van Dishoeck, E. E., *Ann. Rev. Astro. Astrophys.* **2009**, *47*, 427.

[29] Horn A. et al., *Astrophs. J.* **2004**, *611*, 605.

[30] Geppert, W. D. et al., *Faraday Discuss.* **2006**, *133*, 177.

[31] Garrod, R. T. et al., *Faraday Discuss.* **2006**, *133*, 51.

[32] Garrod, R. T., Widicus Weaver, S. L., and Herbst, E., *Astrophs. J.* **2008**, *682*, 283.

[33] Snyder, L. E., *Proc. Nat. Acad. of Sci.* **2006**, *103*, 12243.

[34] Rodríguez-Fernández et al., *Astron. & Astrophys.* **2000**, *356*, 695.

[35] Requena-Torres, M. A., Martín-Pintado, J., Rodríguez-Franco, A., Martín, S., Rodríguez-Fernández, N. J., and de Vincente, P., *Astron. & Astrophys.* **2006**, *455*, 971.

[36] Nummelin et al., *Astrophys. J. Suppl.* **1998**, *117*, 427.

[37] http://www.iram.fr/IRAMFR/GILDAS

[38] Arce et al. *Astrophys. J. Lett.* **2008**, *681*, L21-L24.

[39] Duncan, M., *Private Communication* **2010**.

[40] Kaur et al., *Appl. Opt.* **1990**, *29*, 119.

[41] Lang, S. L., McGuire, B.A., and Widicus Weaver, S. L., "Taking the submillimeter spectrum of an ion." **2011** (Poster).